Behavioral/Cognitive

Anterior–Posterior Hippocampal Dynamics Support Working Memory Processing

Jin Li (李瑾),[1,2*] Dan Cao (曹 丹),[1,2*] Vasileios Dimakopoulos,[3] Weiyang Shi (时维 阳),[1,2,4] Shan Yu (余 山),[1,2,4,5] Lingzhong Fan(樊令 仲),[1,2,4,5] Lennart Stieglitz,[3] Lukas Imbach,[6] Johannes Sarnthein,[3,7] and Tianzi Jiang (蒋田 仔)[1,2,4,5,8]

[1]Brainnetome Center, Institute of Automation, Chinese Academy of Sciences, Beijing 100190, People's Republic of China, [2]National Laboratory of Pattern Recognition, Institute of Automation, Chinese Academy of Sciences, Beijing, 100190, People's Republic of China, [3]Department of Neurosurgery, University Hospital Zurich, University of Zurich, 8091 Zurich, Switzerland, [4]School of Artificial Intelligence, University of Chinese Academy of Sciences, Beijing 100049, People's Republic of China, [5]Center for Excellence in Brain Science and Intelligence Technology, Chinese Academy of Sciences, Beijing 100190, People's Republic of China, [6]Swiss Epilepsy Center, 8008 Zurich, Switzerland, [7]Zurich Neuroscience Center, ETH Zurich, 8057 Zurich, Switzerland, and [8]The Queensland Brain Institute, University of Queensland, Brisbane, Queensland 4072, Australia

The hippocampus is a locus of working memory (WM) with anterior and posterior subregions that differ in their transcriptional and external connectivity patterns. However, the involvement and functional connections between these subregions in WM processing are poorly understood. To address these issues, we recorded intracranial EEG from the anterior and the posterior hippocampi in humans (seven females and seven males) who maintained a set of letters in their WM. We found that WM maintenance was accompanied by elevated low-frequency activity in both the anterior and posterior hippocampus and by increased theta/alpha band (3–12 Hz) phase synchronization between anterior and posterior subregions. Cross-frequency and Granger prediction analyses consistently showed that the correct WM trials were associated with theta/alpha band-coordinated unidirectional influence from the posterior to the anterior hippocampus. In contrast, WM errors were associated with bidirectional interactions between the anterior and posterior hippocampus. These findings imply that theta/alpha band synchrony within the hippocampus may support successful WM via a posterior to anterior influence. A combination of intracranial recording and a fine-grained atlas may be of value in understanding the neural mechanisms of WM processing.

Key words: **hippocampus; intracranial EEG; longitudinal axis; working memory**

Significance Statement

Working memory (WM) is crucial to everyday functioning. The hippocampus has been proposed to be a subcortical node involved in WM processes. Previous studies have suggested that the anterior and posterior hippocampi differ in their external connectivity patterns and gene expression. However, it remains unknown whether and how human hippocampal subregions are recruited and coordinated during WM tasks. Here, by recording intracranial electroencephalography simultaneously from both hippocampal subregions, we found enhanced power in both areas and increased phase synchronization between them. Furthermore, correct WM trials were associated with a unidirectional influence from the posterior to the anterior hippocampus, whereas error trials were correlated with bidirectional interactions. These findings indicate a long-axis specialization in the human hippocampus during WM processing.

Received June 22, 2021; revised Nov. 4, 2021; accepted Nov. 11, 2021.

Author contributions: J.S. and T.J. designed research; V.D., L.S., and L.I. performed research; J.L. and D.C. analyzed data; J.L., D.C., V.D., W.S., S.Y., L.F., J.S. and T.J. wrote the paper.

This work received support from the following sources: National Key Research and Development Program of China (2017YFA0105203); the Chinese Academy of Sciences Science and Technology Service Network Initiative (Grant KFJ-STS-ZDTP-078); National Natural Science Foundation of China (Grants 31300934 and 31620103905); Science Frontier Program of the Chinese Academy of Sciences (Grant QYZDJ-SSW-SMC019); the National Key R&D Program of China (Grant 2017YFA0105203); Open Research Fund of the State Key Laboratory of Cognitive Neuroscience and Learning (Grant CNLYB2004); Open Research Fund of the CAS Key Laboratory of Behavioral Science, the Institute of Psychology; and the Swiss National Science Foundation (Grant SNSF 176222 to J.S.). We thank Prof. Yuanye Ma from the Key Laboratory of External Drug Delivery System and Preparation Technology in the University of Yunnan Province, and the School of Chinese Materia Medica, Yunnan University of Chinese Medicine for suggestions. We also thank Dr. Rhoda E. Perozzi and Dr. Edmund F. Perozzi for English and content editing assistance.

*J.L. and D.C. contributed equally to this work.

The authors declare no competing financial interests.

Correspondence should be addressed to Tianzi Jiang at jiangtz@nlpr.ia.ac.cn or Johannes Sarnthein at johannes.sarnthein@usz.ch.

https://doi.org/10.1523/JNEUROSCI.1287-21.2021

Introduction

Working memory (WM), the "sketchpad of conscious thought" (Miller et al., 2018), is critical for organizing goal-directed behaviors (D'Esposito, 2007). It describes our capacity to temporarily hold information and adaptively translate it later into a behavioral response. The hippocampus (Hipp) has been proposed to be a subcortical node underlying WM. Direct electrophysiological recordings in the human hippocampus consistently found persistent single-neuron activity (Kamiński et al., 2017; Kornblith et al., 2017; Boran et al., 2019), power change (Brzezicka et al., 2019), and increased phase–amplitude coupling (PAC; Axmacher et al., 2010) during WM maintenance. These studies modeled the hippocampus as a single, homogeneous entity; however, the hippocampus is a complex, heterogeneous structure consisting of distinct, interacting subregions. Rodent studies suggested that the ventral (homologous to the anterior in humans) and dorsal (homologous to the posterior in humans) hippocampi differ in their connectivity and gene expression patterns (Fanselow and Dong, 2010; Poppenk et al., 2013). Such connectivity and transcriptomic heterogeneity have recently been validated in humans (Vos de Wael et al., 2018; Vogel et al., 2020) and provide a rationale for the functional differentiation along the long axis (Poppenk et al., 2013; Strange et al., 2014). Consistent with this hypothesis, Lin et al. (2017, 2019) reported that during episodic memory encoding, the positive subsequent memory effect in the slow-theta range is greater in the posterior hippocampus (Lin et al., 2017); later, they found that gamma activity was greater during retrieval than during encoding only in the posterior hippocampus (Lin et al., 2019). Given that mounting evidence shows functional organization along the longitudinal axis, treating the hippocampus as a functionally uniform structure in WM processing may disregard potentially useful information about its subregions.

Rodent experiments suggested a critical role of the dorsal but not the ventral hippocampus in WM processing, with a significant WM deficit caused by dorsal but not ventral hippocampal lesions (Pothuizen et al., 2004). A recent meta-analysis of functional magnetic resonance imaging (MRI) studies involving humans reported activation of both the anterior Hipp (aHipp) and the posterior Hipp (pHipp) during WM processing (Grady, 2020). The limited temporal and spatial resolution of this noninvasive MRI technique in human studies has made it difficult to capture the functional specialization of the hippocampus at a fine-grained scale. Thus, direct brain recordings precisely located in hippocampal subregions during WM tasks are required. In addition, the anatomic connectivity suggests a flow of information between the aHipp and the pHipp (Schmidt et al., 2013). Rodent studies showed increased connectivity between the dorsal and ventral hippocampi as they engage in WM processing (Schmidt et al., 2013). However, it remains unknown whether and how the two hippocampal subregions communicate during WM in humans. Human intracranial electroencephalography (iEEG) recordings, with both millimeter spatial precision and millisecond temporal resolution, even in deep brain regions (Johnson et al., 2020), offer the possibility of delineating activity at the hippocampal subregion level and of studying the information flow between the two hippocampal subregions *in vivo* (Lin et al., 2017).

Here, we recorded iEEG simultaneously from the aHipp and the pHipp in 14 presurgical epilepsy patients while they performed a modified Sternberg task. We addressed the following questions. (1) Does the hippocampus play a single role in WM processing or is there spatial heterogeneity along the long axis in its involvement in working memory? (2) Are the aHiPP and the pHipp independent or do they interact in WM? (3) Do these activities or interactions support WM maintenance?

Materials and Methods

Subjects. We used data from 14 adult human subjects (mean ± SD age, 32 ± 12 years; age range, 18–56 years; seven males) in this study. All subjects were implanted with depth electrodes [diameter, 1.3 mm; 8 contacts of 1.6 mm length; 5 mm spacing between contact centers; Ad-Tech (www.adtechmedical.com)] in the medial temporal lobe for evaluation of the surgical treatment of epilepsy. Electrode placement was exclusively guided by clinical needs, and patient selection was based on MRI-confirmed depth electrode placement in the hippocampus contralateral to or outside of the epileptogenic region. Before testing, all the subjects provided written informed consent for the study, which had been approved by the relevant institutional ethics review board (Kantonale Ethikkommission Zürich, Approval PB 2016–02055). There were no seizures recorded during any of the epochs, and any epochs with interictal epileptiform activity were excluded from analysis.

Experimental design and statistical analyses. WM was tested using a modified Sternberg task in which the encoding of memory contents, maintenance, and recall were temporally separated (Fig. 1*A*). Each trial started with a fixation period (1 s) followed by the stimulus for 2 s. The memory content consisted of a set of letters at the center of the screen. After the disappearance of the stimulus, the maintenance interval was followed by a fixation square (3 s). After that, the subjects responded with a button press ("IN" or "OUT") as fast as possible when a probe was presented. They were instructed to recall whether the probe was part of the stimulus. After the response, the subjects were encouraged to relax, and the next trial was initiated. Each subject performed several sessions with 50 trials per session (226 ± 113 trials per subject), and the order of the stimuli was fully random across sessions.

We then statistically compared the *z*-scored power between the aHipp and the pHipp using a cluster-based permutation test, which computes statistics at the cluster level and corrects for multiple comparisons (Maris and Oostenveld, 2007). The differences between the aHipp and the pHipp were quantified by *t* values. The *t* values corresponding to uncorrected *p* values of ≤ 0.05 were clustered. The differences were considered significant when the maximum of the cluster-level summed *t* values in the true data exceeded the threshold of a Monte Carlo distribution, which was created by randomly shuffling the labels of the outcomes 1000 times, and $p < 0.05$ was considered as significant. Such a comparison was also applied in the phase–amplitude coupling analysis to assess the task-induced effects from the maintenance period over the baseline ($p < 0.05$). In addition, we examined the statistical significance of the phase locking values (PLVs) of the aHipp–pHipp electrode pairs by permuting the trials 200 times to create a null distribution and computed the 95th percentile threshold for each pair. The PLVs above the thresholds were considered to be significant ($p < 0.05$). A similar permutation test was also applied on the Granger causality (GC) analysis. We used mixed-effect models (MEMs) to compare the electrophysiological indexes for two directions of information transfer between the aHipp and the pHipp. All data analyses were conducted using MATLAB (MathWorks).

Depth electrode localization. The electrodes were localized using postimplantation computed tomography (CT) scans and postimplantation structural T1-weighted MRI scans. For each subject, the CT scan was coregistered to the postimplantation scan, as implemented in FieldTrip (Oostenveld et al., 2011). The electrode contacts were visually marked on the coregistered CT-MR images. To determine the electrode locations, we used a high-resolution anatomic template (1 mm) developed in our laboratory (Fan et al., 2016), which parcellates the brain into 246 subregions based on their anatomic connectivity patterns. This template has been widely used in past studies (Stolk et al., 2018; Assaneo et al., 2019; Lee et al., 2021). In this atlas, the hippocampus is divided into anterior and posterior subregions along the long axis (http://atlas.brainnetome.org/).

The final dataset contained 94 contacts in the hippocampus including 32 contacts in the aHipp and 62 contacts in the pHipp across all

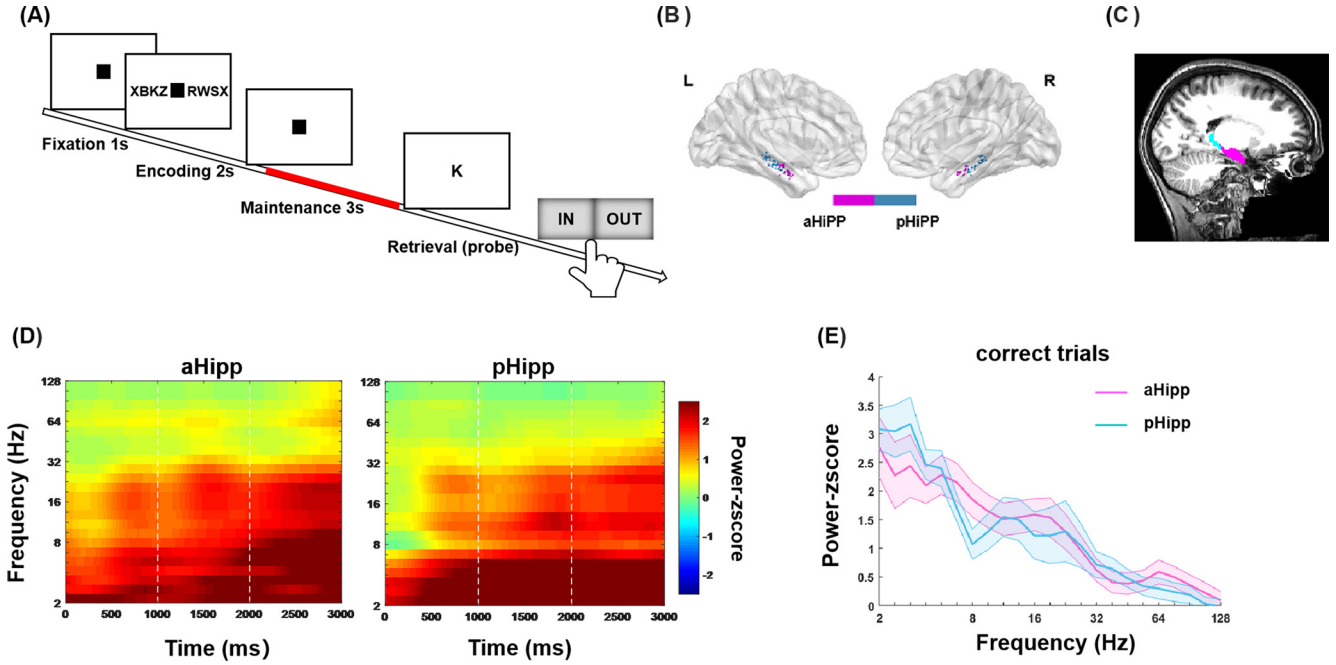

Figure 1. Working memory task, recording sites in the hippocampus, and time–frequency power. ***A***, An example trial of the task. Each trial consisted of a set of consonants (encoding, 2 s), followed by a delay (maintenance, 3 s). After the delay, a probe letter was shown, and the subjects indicated whether the probe was or was not shown during the encoding period (retrieval, 2 s). ***B***, Electrode location across subjects in Montreal Neurologic Institute (MNI152) space. Recording subregions are indicated by different colors (magenta, aHipp; cyan, pHipp). ***C***, An example MRI and template for a single subject. ***D***, Average task-induced power, grouped in the anterior hippocampus (left column) and posterior hippocampus (right column), across all subjects during the maintenance phase for the correct trials. Warmer colors denote task-increased power above the baseline, and colder colors denote task-decreased power. Both the aHipp and the pHipp showed sustained task-increased power in the low-frequency range (2–20 Hz; $z > 1.96$, $p < 0.05$) during the maintenance phase. ***E***, Spectral *z*-scored power within the anterior (magenta) and posterior hippocampus (cyan) across all subjects (±SEM shown as shading around the mean trace) for the correct trials. During maintenance, no significant difference in the spectral power ($p > 0.05$, cluster-based permutation test) was found between the two subregions across the frequency band.

subjects. There were 3.2 ± 1.8 contacts per subject in the aHipp (range, 1–6; 10 of 14 subjects) and 6.7 ± 2.2 contacts per subject in the pHipp (range, 1–8). Thus, the data from 10 subjects with electrodes in both the aHipp and the pHipp were included in the interregional connectivity analysis. Figure 1*B* presents the electrodes transformed into standard MNI space in the aHipp and pHipp across all subjects.

Data acquisition and preprocessing. Intracranial data were acquired using a Neuralynx ATLAS recording system, sampled at 4 kHz, and analog filtered >0.5 Hz against a common intracranial reference. After data acquisition, neural recordings were downsampled to 1 kHz and bandpass filtered from 1 to 200 Hz using the zero-phase delay FIR (finite impulse response) filter with Hamming window. Line noise harmonics were removed using a discrete Fourier transform. The filtered data were manually inspected to mark any contacts or epochs containing epileptiform activity or artifacts for exclusion. The data were then rereferenced to the average of the signal over all the contacts. The contacts localized in the hippocampus were then selected for subsequent analysis. Channels were excluded when they had continuous artifacts, usually because the cable was broken. In our analysis, only one contact was excluded for this reason. In addition, for all the participants, 1.4% of the trials ($n = 43/3050$) were excluded because of large singular artifacts, usually because the cable moved.

The continuous data were segmented into 8 s trials with a 1 s fixation period as the baseline, 2 s encoding period, 3 s maintenance period, and 2 s retrieval period. We focused on the maintenance period. The trials with residual artifacts were rejected via visual inspection. The subjects' responses defined correct and incorrect trials. Preprocessing routines were performed using the FieldTrip (Oostenveld et al., 2011), EEGLAB (Delorme and Makeig, 2004) toolboxes and customized scripts for MATLAB.

Frequency decomposition. Time–frequency representations of power were computed for correct and incorrect trials. For each trial for each electrode, we convolved the signal within the aHipp and the pHipp with complex-valued Morlet wavelets (six cycles) to obtain power information (Solomon et al., 2019). The frequency range was 2–128 Hz at 23 logarithmically spaced frequencies with a time resolution of 1 ms. The task-induced power was analyzed per trial using the same statistical bootstrapping procedure as used in previous studies (Johnson et al., 2018). Briefly, for each channel and frequency, the baseline power (500 ms pretrial) was pooled into a single time series; then *r* data points (r = number of trials of the subject) were randomly selected and averaged. This procedure was repeated 1000 times to create a null distribution. The raw power for each time point was then *z*-scored by comparing it to the entire null distribution. The task-induced power was considered significant when the *z*-scored power exceeded the value of 1.96 ($p < 0.05$). Then, the *z*-scored power for the aHipp and the pHipp was compared at each time–frequency point with a cluster-based permutation test (Maris and Oostenveld, 2007) for the correct and the incorrect trials, separately.

Interregional phase synchrony. The strength of the interregional neural synchrony was quantified by the PLV, which calculates the average phase φ difference between two electrodes (a,b) across trials for a given time point t and frequency f, as follows:

$$\mathrm{PLV}_{a,b}(t,f) = \frac{1}{N\mathrm{trials}}\left|\sum_{n=1}^{n=N\mathrm{trials}} \exp\left(i\left[\varphi_{\mathrm{n,a}}(t,f) - \varphi_{\mathrm{n,b}}(t,f)\right]\right)\right|. \quad (1)$$

The PLV indexes the degree of consistency of the phase relationship for each pair of electrodes independent of the absolute phases and amplitudes among repeated trials and ranges from 0 to 1, with values approaching 1 if the two signals show a constant phase relationship. We calculated the PLV for each electrode pair of the aHipp–pHipp from 1 to 30 Hz across the correct and the incorrect trials, separately. The trialwise mean was subtracted from each trial to minimize contamination from simultaneous voltage changes of the phase estimates before calculating the PLV (Brincat and Miller, 2015).

To test the statistical significance of the PLVs of all electrode pairs within the maintenance trials, we permuted the trials 200 times to create a null distribution and computed the 95th percentile threshold for each pair. The thresholds were then averaged across all electrode pairs and only the time–frequency PLVs above the corresponding thresholds were kept as significant PLVs. The values below the thresholds were set to zero. To further specify the frequency-specific PLVs, the spectral PLVs were obtained across time. We selected and extracted the peak PLVs (theta/alpha, 3–12 Hz) to compare the PLVs with the baseline using a paired *t* test to confirm that this peak was associated with the maintenance process.

Granger causality analysis. To examine the directionality of the aHipp–pHipp synchronization within the theta/alpha band, we analyzed the effective aHipp–pHipp connectivity using spectral GC, which quantifies the prediction error of the signal in the frequency domain by introducing another time series. Based on observations from previous studies (Kota et al., 2020), we extracted the GC values within 3–12 Hz that showed task-related elevated PLV. The aHipp–pHipp electrode pairs with task-induced elevated connectivity (theta/alpha PLVmaintenance/PLVbaseline > 1) for the correct and incorrect trials were selected separately. Following this criterion, 49 of 84 electrode pairs for correct trials and 40 pairs for incorrect trials were selected separately for later analysis. For each electrode pair of the aHipp–pHipp, the trialwise mean was subtracted from each trial before being fit to an autoregressive model and computing the spectral GC. We then applied the Multivariate Granger Causality MATLAB Toolbox (Barnett and Seth, 2014) based on the Akaike information criterion to define the model order for each pair. The GC index of both directions (from aHipp to pHipp and the reverse direction) was computed during the maintenance period for the correct and incorrect trials, separately. The significance testing for the spectral GC was conducted by creating a null distribution by randomly swapping the signal between the electrodes 200 times. The electrode pairs with a GC above the threshold, defined as the 95th percentile of the null distribution, were selected for the subsequent comparisons.

The theta/alpha GC for each pair was extracted in both directions for the correct trials and the incorrect trials, separately. Then, two MEMs were used to compare the GC value from both directions, for the correct and incorrect trials. In each MEM, we treated the direction as a fixed factor, the electrode pair number and subjects as random factors, and the extracted theta/alpha GC values for each electrode pair as the dependent variables.

Given that the GC analysis is sensitive to the signal-to-noise ratio across frequency bands, we also assessed the theta/alpha band directionality using the phase slope index (PSI; Basti et al., 2018) from both directions for the correct and incorrect trials, separately. Again, the electrode pairs with elevated PLVs for the correct and incorrect trials were selected separately. For each trial, the data segments during maintenance were zero padded and multiplied with a Hann taper from 3 to 12 Hz with 1 Hz steps, from which we computed the theta/alpha PSI (Johnson et al., 2018). To correct for any spurious results, null distributions were generated by randomly shuffling the trials 1000 times. Raw PSI outputs were then *z*-scored on the null distributions to assess the significance of the directional effects. Significant PSI was thresholded at $|z| > 1.96$, in which the aHipp leads were defined as $z > 1.96$ and the pHipp leads as $z < -1.96$.

Phase–amplitude coupling. The cross-frequency coupling between the lower frequency (1–20 Hz) phase from contact *a* and the higher-frequency (20–100 Hz) amplitude from contact *b* was examined individually by mean vector length (Canolty et al., 2006). Phase–amplitude coupling was calculated according to the following equation:

$$PAC = \left| \frac{\sum_{t=1}^{n} A_{t,a} e^{i\varphi_{t,b}}}{n} \right|, \quad (2)$$

where n is the number of data points, t is a data point, $A_{t,a}$ is the amplitude, and $\varphi_{t,b}$ is the phase angle.

Then, the raw PAC was assessed against surrogate distributions via bootstrapping as was done in previous studies (Canolty et al., 2006). Specifically, we shuffled data by inserting a randomly generated time lag between the time series of the low-frequency phase and the high-frequency amplitude and recomputed the PAC. This procedure was repeated 200 times to create surrogate distributions of PAC values. Then, the raw PAC was *z*-scored based on the null distributions to correct for any spurious results. The *z*-scored PACs exceeding a threshold value of 1.96 were considered as significant (Wang et al., 2021). To assess the task-induced effects, the *z*-scored PAC during the maintenance was compared with the baseline values by the cluster-based permutation test used in the previous analysis. A one-tailed test was applied to find the task-increased coupling relative to the baseline ($p < 0.05$).

We extracted the theta/alpha (3–12 Hz)–gamma (30–100 Hz) *z*-scored PAC from the following two directions: the theta/alpha phase of the aHipp modulating the gamma amplitude of the pHipp as well as the theta/alpha phase of the pHipp modulating the gamma amplitude of the aHipp for the correct and incorrect trials, separately. The outputs were analyzed using an MEM, with direction as a fixed factor, subject and electrode pair as random factors, and *z*-scored PAC for each electrode pair as a dependent variable.

Data and code availability. The dataset has been analyzed and described previously (Boran et al., 2019, 2020, 2021) and is freely available for download at https://doi.gin.g-node.org/10.12751/g-node.d76994/. The task is freely available for download at http://www.neurobs.com/ex_files/expt_view?id=266. Links to updates and further datasets can be found at https://hfozuri.ch.

Results

Task and behavior

Fourteen presurgical epilepsy patients (7 males; Table 1) performed a modified Sternberg WM task (58 total sessions from 14 subjects). In this task, items were presented simultaneously rather than sequentially, thus separating the encoding stage from the maintenance stage. In each trial, the subject was asked to memorize a set of 4, 6, or 8 letters presented for 2 s (encoding). After a delay (maintenance) period of 3 s, the subjects were instructed to judge whether a probe letter was identical to one of the letters held in memory (retrieval; Fig. 1*A*).

The average accuracy was 90.8 ± 1.2% (range, 78−94.9%). The mean response time was faster for correct than incorrect trials (1.32 ± 0.04 vs 1.81 ± 0.15 s; paired *t* test: $t_{(13)} = -4.0489$, $p = 0.0005$). Hence, the subjects were able to perform the WM task.

Low-frequency activity is sustained during maintenance

Local field potentials were recorded from the depth electrodes implanted in the aHipp (32 contacts) and the pHipp (62 contacts; Fig. 1*B*). The average distance between the anterior and posterior contacts was 19.59 ± 0.80 mm (range, 4.69–36.67 mm). An example MRI and template were also presented for a single subject (Fig. 1*C*). We calculated the time–frequency power for the correct trials/for each contact in each of the subregions during the maintenance period, and the power outputs were *z*-scored against pretrial baseline distributions to assess the significance of the task-induced power effects per trial. Both the aHipp and the pHipp showed sustained activity in the low-frequency range (2–20 Hz; $z > 1.96$, $p < 0.05$; Fig. 1*D*). Then we averaged the spectral power across time and compared it between the aHipp and the pHipp at each frequency. We found no aHipp–pHipp difference in the spectral power ($p > 0.05$, clustered-based permutation test) across the frequency bands for the correct trials (Fig. 1*E*). Together, both the aHipp and the pHipp engaged in the maintenance of the WM information, as reflected by the low-frequency oscillations.

Table 1. Subject characteristics

Subject	Age (years)	Gender	Recording sites (aHipp)	Recording sites (pHipp)	Retrieval accuracy	RT for correct trials (mean ± SD)
1	24	Female	2	2	0.925	1.26 ± 0.63
2	39	Male	0	3	0.864	1.28 ± 0.65
3	18	Female	2	6	0.932	1.10 ± 0.34
4	28	Male	1	6	0.9492	1.48 ± 0.63
5	20	Female	3	2	0.913	1.41 ± 0.90
6	31	Male	6	7	0.943	1.47 ± 0.59
7	47	Male	5	8	0.949	1.44 ± 0.57
8	56	Female	1	5	0.900	1.41 ± 0.51
9	19	Female	4	8	0.928	1.24 ± 0.33
10	31	Female	2	2	0.780	1.22 ± 0.42
11	35	Male	0	5	0.930	1.64 ± 0.73
12	20	Male	0	4	0.925	1.11 ± 0.32
13	19	Male	0	1	0.863	1.18 ± 0.42
14	51	Female	6	4	0.914	1.30 ± 0.58

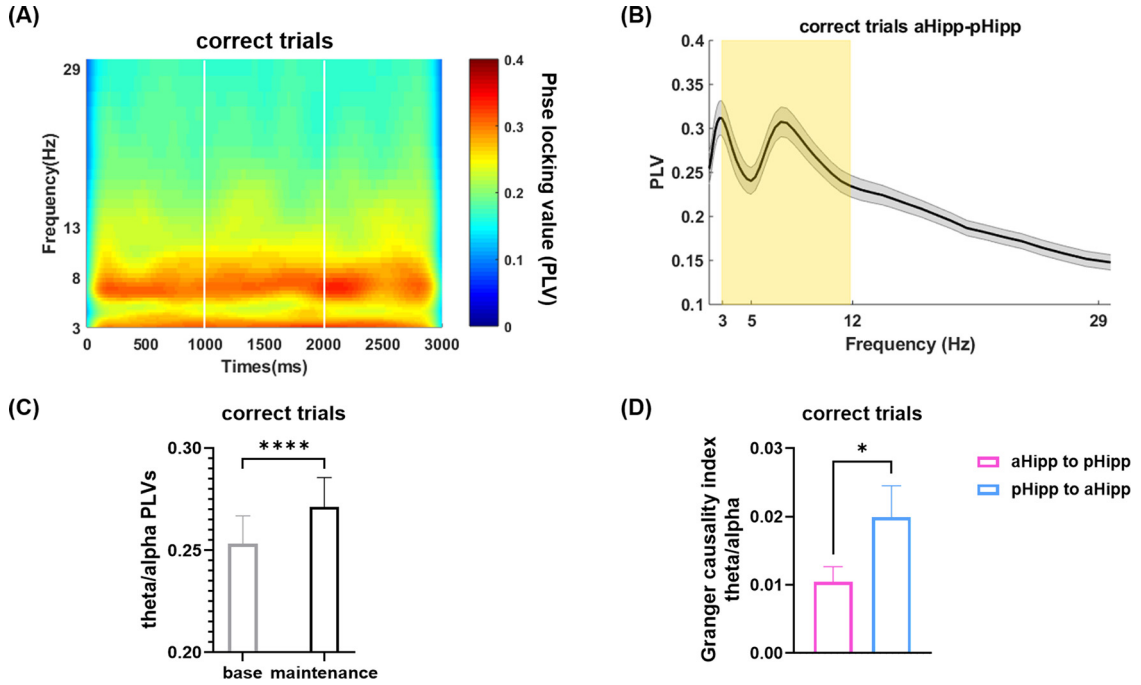

Figure 2. Frequency-specific aHipp–pHipp phase synchrony during maintenance. ***A***, Phase synchrony (PLV) between the anterior hippocampus and the posterior hippocampus was identified across all subjects, with greater theta/alpha synchrony during the maintenance for the correct trials. The PLVs ranged from 0 to 1, with warmer colors indicating greater PLVs. The PLV maps show the PLVs that survived the threshold at $p < 0.05$ (cluster-based permutation test). ***B***, Spectral PLVs within 1–30 Hz between the aHipp and the pHipp across subjects for the correct trials (±SEM shown as shaded area around the mean trace) with peaks in the theta/alpha band (3–12 Hz, shading in light orange). The shaded area indicates the theta/alpha range used for the subsequent analyses. ***C***, Extracted theta/alpha PLVs of the aHipp–pHipp across all subjects for the baseline and maintenance in the correct trials. The theta/alpha PLVs were elevated by the maintenance relative to the baseline (paired *t* test, $t_{(83)} = 3.97$, $p = 0.0002$). ***D***, The GC index for the correct trials was extracted within the theta/alpha band across subjects for two directions (magenta: aHipp to pHipp; cyan: pHipp to aHipp). Stronger GC was found for pHipp to aHipp (cyan) than for aHipp to pHipp (magenta; mixed-effect model, $^*p < 0.05$).

Theta/alpha synchronization of aHipp–pHipp supports the maintenance of WM information

Task-induced increases in spectral power were found within the low-frequency bands for both the aHipp and the pHipp. This raised a further question about whether the two subregions of the hippocampus interact during WM maintenance. Given the role of low-frequency oscillations in supporting interregional communication, we calculated the low-frequency phase synchrony with PLVs between the aHipp and the pHipp for the correct trials, thus measuring the consistency of the phase relationship for each aHipp–pHipp electrode pair. The PLVs up to 30 Hz were computed across the time–frequency domain to reveal the dynamic fluctuations throughout the functional connectivity during the maintenance period. This analysis was done using the data from 10 participants who had electrodes in both the anterior and the posterior hippocampi.

As shown in Figure 2*A*, evident phase synchronization ($p < 0.05$, permutation test) between aHipp and pHipp was found throughout the entire maintenance period. Further, we obtained the spectral PLVs across the time domain and confirmed that the PLVs of aHipp–pHipp peaked in the theta/alpha band (3–12 Hz; Fig. 2*B*, light orange shadowed). To confirm whether this peak in the PLVs was maintenance related, we extracted the PLVs within the theta/alpha band for the maintenance period and the baseline fixation, and compared them using a paired *t* test. For all the aHipp–pHipp electrode pairs, the PLVs for the maintenance phase were significantly stronger than those for the baseline fixation (paired *t* test: $t_{(83)} = 3.97$,

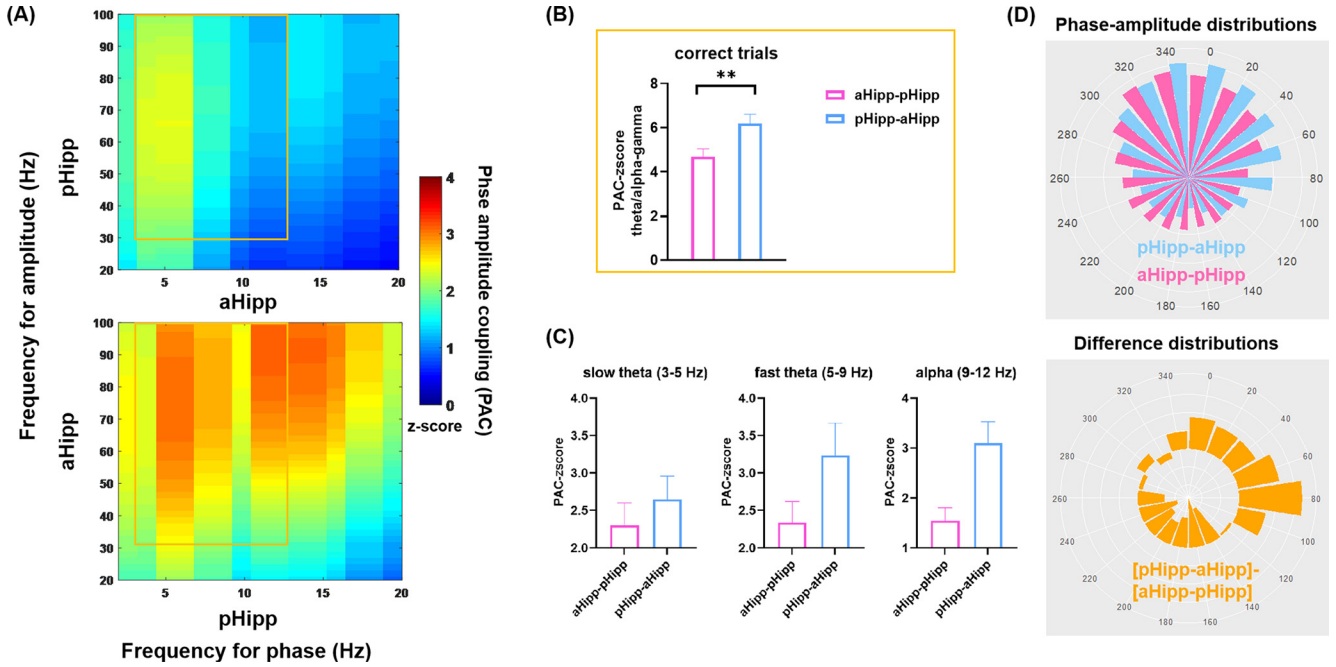

Figure 3. Cross-frequency coupling between the aHipp and the pHipp. ***A***, Average cross-frequency phase–amplitude coupling (*z* score) between the anterior hippocampus and posterior hippocampus across all subjects for correct trials. To assess the task-induced effects, the *z*-scored PAC during the maintenance was compared with the baseline values by the cluster-based permutation test. A one-tailed test was applied to find the task-increased coupling relative to the baseline ($p < 0.05$). For the theta–alpha phase (3–12 Hz)/gamma amplitude (30–100 Hz) coupling shown in the orange boxes, interregional modulations for both directions were significantly higher during maintenance relative to those in the baseline period (all *p* values < 0.05). ***B***, The theta/alpha–gamma (orange box) PACs were calculated across subjects for two directions (magenta, aHipp–pHipp means aHipp phase modulating pHipp amplitudes; cyan, pHipp–aHipp means the reverse direction) for the correct trials. The modulation strength from the pHipp to the aHipp was greater than that from the aHipp to the pHipp (mixed-effect model, $^{**}p < 0.01$). ***C***, Average *z*-scored intrahippocampal PAC for the slow-theta (3–5 Hz)–gamma, fast-theta (5–9 Hz)–gamma, and alpha (9–12 Hz)–gamma PACs between the aHipp and the pHipp in both phase–amplitude combinations (low-frequency phase from the aHipp and alpha amplitude from the pHipp, and vice versa). For each frequency band, the coupling strength between the pHipp phase and the aHipp amplitude (pHipp–aHipp, cyan) was consistently greater than that between the aHipp phase and the pHipp amplitude (aHipp–pHipp, magenta). ***D***, Computation of theta/alpha–gamma interactions. Phase–amplitude distributions were constructed for both directions (top: magenta, gamma amplitudes of the pHipp distributed across the theta/alpha phase bins of the aHipp, abbreviated as aHipp–pHipp; cyan, gamma amplitudes of the aHipp distributed across the theta/alpha phase bins of the pHipp, abbreviated as pHipp–aHipp). The difference distributions were obtained by subtracting the aHipp–pHipp from the pHipp–aHipp (bottom, orange). The gamma activity from both the aHipp (magenta) and the pHipp (cyan) was modulated by the theta/alpha oscillations around the trough (Rayleigh test, average pHipp gamma amplitude occurred at 57.3°, $p_{pHipp} = 4.31 \times 10^{-8}$; average aHipp gamma amplitude occurred at 57.2°, $p_{aHipp} = 4.31 \times 10^{-8}$). The difference distributions were not uniform (Rayleigh test, $p = 4.31 \times 10^{-8}$).

$p = 0.0002$), confirming that the peak of the PLVs within the theta/alpha band was strongly associated with the maintenance process (Fig. 2*C*). Therefore, the subsequent analyses focused on the theta/alpha band.

pHipp drives aHipp in the theta/alpha band supporting WM processing

To further examine the directionality of the aHipp–pHipp synchronization within the theta/alpha band, we analyzed the effective aHipp–pHipp connectivity using GC in the frequency domain. GC estimates the degree to which the signal from one region can be predicted by incorporating information from another. Next, we compared the GC values in the pHipp-to-aHipp direction with those from the reverse direction. We found that the theta/alpha-driven GC values were greater in the pHipp-to-aHipp direction than those in the reverse direction (mixed-effect model: $t = 2.10$, $p = 0.039$; Fig. 2*D*). These results provided evidence that directional aHipp–pHipp interactions driven by the pHipp in the theta/alpha band supported successful WM processing.

In addition to the GC analysis, we assessed the theta/alpha band directionality between the aHipp and the pHipp by calculating the PSI within the theta/alpha band (3–12 Hz). We found a unidirectional pHipp-driven connectivity ($z = -2.78$, $p = 0.0054$) for the correct trials and bidirectional aHipp–pHipp interactions ($z = 0.89$, $p = 0.37$) for incorrect trials in the theta/alpha band. This result confirmed the result from the GC analysis, and together they indicated that pHipp-driven information flow supports successful WM processing.

Cross-frequency information transfer between the aHipp and the pHipp

PAC serves as an important mechanism for coordinating interregional information transfer in that high-frequency amplitudes are modulated by phases with a low frequency (Canolty et al., 2006). It has been suggested that PAC, especially theta/alpha-gamma PAC within the hippocampus, reflects a neural correlate for WM maintenance in animals and humans (Tort et al., 2008; Axmacher et al., 2010; Roux and Uhlhaas, 2014). We computed the cross-regional PAC in both phase–amplitude combinations between the aHipp and the pHipp for the correct trials. The interregional influence was quantified as the coupling of low-frequency phases (2–20 Hz; Martínez-Cancino et al., 2019) from one region with high-frequency amplitudes (20–100 Hz) to another. The raw PAC was *z*-scored against surrogate distributions via bootstrapping. The results showed that the theta/alpha phase of the aHipp entrained the gamma amplitude of the pHipp (~30–100 Hz; peak, 78 Hz; Fig. 3*A*, top) and the theta/alpha phase of the pHipp modulated the gamma amplitude of the aHipp (~30–100 Hz; peak, 80 Hz; Fig. 3*A*, bottom). To further

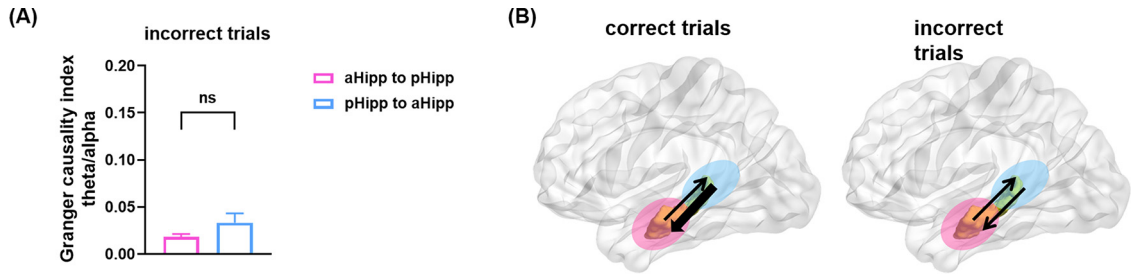

Figure 4. Directionality of the aHipp–pHipp for the incorrect trials. ***A***, The GC index for the incorrect trials was extracted within the theta/alpha band across subjects for two directions (magenta, aHipp to pHipp; cyan, pHipp to aHipp). No difference in GC was found between the aHipp and the pHipp for either direction (mixed-effect model, $p > 0.05$). ***B***, Schematics of the maintenance of WM processing within the hippocampus for the correct trials (left) and the incorrect trials (right). Directional information flow driven by the pHipp to the aHipp within the theta/alpha band subserved the correct performance in the WM trial, but this bias with respect to the directionality of information transfer was absent in incorrect WM trials.

compare the coupling strength between the two combinations, the cross-regional PAC of the theta/alpha–gamma bands (Fig. 3*A*, orange box) was extracted for both combinations. We found that the coupling strength between the pHipp phase and the aHipp amplitude was greater than that between the aHipp phase and the pHipp amplitude (mixed-effect model, $t = 2.84$, $p = 0.006$), as shown in Figure 3*B*.

Based on previously reported aHipp/pHipp differences in preferred frequencies of the hippocampal cortex PAC in episodic memory processing (Wang et al., 2021), we further divided the theta/alpha band (3–12 Hz) into three frequency bands in our PAC analysis. We separately extracted the phase information for the slow-theta (3–5 Hz), fast-theta (5–9 Hz), and alpha (9–12 Hz) frequency bands in one hippocampal subregion and the amplitude information for the gamma band in the other hippocampal subregion. Then, the raw PAC outputs were *z*-scored against surrogate distributions. The coupling strength between the pHipp phase and the aHipp amplitude was consistently greater than that between the aHipp phase and the pHipp amplitude for these frequency bands (Fig. 3*C*). These results further demonstrated that the pHipp slow oscillations consistently directed the aHipp gamma during working memory processing.

Low-frequency oscillations are thought to organize cell assemblies to maintain WM information, and recent studies indicate that neuronal spiking in the hippocampus is locked to distinct phases of slow oscillations in a behaviorally relevant manner (Kamiński et al., 2020). As a surrogate for neuronal spiking, we examined when gamma activity from the modulated signals occurred relative to the theta/alpha phases of the modulating signal. The distributions of the gamma amplitudes across 18 phase bins were calculated for both directions. As shown in Figure 3*D*, top, the gamma activity from both the aHipp (magenta) and the pHipp (cyan) was modulated by the theta/alpha oscillations around the trough (Rayleigh test: average pHipp gamma amplitude occurred at 57.3°, $p_{\mathrm{pHipp}} = 4.3082 \times 10^{-8}$; average aHipp gamma amplitude occurred at 57.2°, $p_{\mathrm{aHipp}} = 4.3085 \times 10^{-8}$). Moreover, the distributions of the gamma amplitudes in the pHipp across the theta/alpha phase bins in the aHipp were subtracted from those of the gamma amplitudes of the aHipp across the theta/alpha phase bins of the pHipp, as shown in Figure 3*D*, bottom. The differences were not uniform (Rayleigh test, $p = 4.308 \times 10^{-8}$). In summary, WM maintenance increased cross-frequency coupling between the aHipp and the pHipp at frequency- and phase-specific oscillations, and the gamma amplitudes during the theta/alpha phase oscillations optimized the information transfer from the posterior to the anterior hippocampus.

Directionality between aHipp and pHipp is unbiased for the incorrect trials

To investigate whether the findings above were specific for successful WM maintenance, we also analyzed the directionality of the information transfer between the aHipp and the pHipp for the incorrect trials. Within the theta/alpha band, significant GC above the threshold was found within the incorrect trials and no difference in GC was found for either direction between the aHipp and the pHipp (mixed-effect model: $t = 1.668$, $p = 0.12$), as shown in Figure 4*A*. To exclude the possibility that the lack of effect of direction for the incorrect trials are because of different electrode pairs used in statistical analysis, we repeated our analysis by using all 84 electrode pairs to compare the GC values from both directions for the correct and incorrect trials, separately. The GC values from pHipp to aHipp were significantly higher than those from the opposite direction (mixed-effect model: $t = 2.06$, $p = 0.043$) for the correct trials, while there was no significant difference between the two directions (mixed-effect model: $t = 0.46$, $p = 0.65$) for the incorrect trials. These results confirmed our findings. Therefore, the directionality of information transfer driven by the pHipp to the aHipp supported WM maintenance (Fig. 4*B*, left), which was beneficial for correct WM performance. However, this bias in the directionality of information transfer was absent in the hippocampus in incorrect trials (Fig. 4*B*, right).

As we did for the analyses conducted for the correct trials, we also computed the time–frequency power during the maintenance period for the incorrect trials within the aHipp and pHipp separately. As shown in Figure 5*A*, task-induced power for the incorrect trials on both the aHipp and the pHipp was not sustained during the maintenance in the low-frequency range (2–20 Hz). The spectral power was not significant ($z < 1.96$) during the maintenance period and no difference ($p > 0.05$, clustered-based permutation test) was found between the two subregions across the frequency band (Fig. 5*B*). In addition, the PLV across the time–frequency domain was also calculated between the aHipp and the pHipp for the incorrect trials. However, only a few scattered PLV points survived significance testing during the maintenance of incorrect trials (Fig. 5*C*). As a result, we did not conduct further analyses on the PLVs for the incorrect trials as we did for the correct trials.

Volume conduction and recording montage

To rule out effects of volume conduction, we repeated our analysis of connectivity and Granger causality after rereferencing our recordings to a bipolar scheme (for a similar approach, see Kota et al., 2020). First, we found sustained phase synchronization ($p < 0.05$, clustered-based permutation test) between aHipp and pHipp in the low-frequency band throughout the

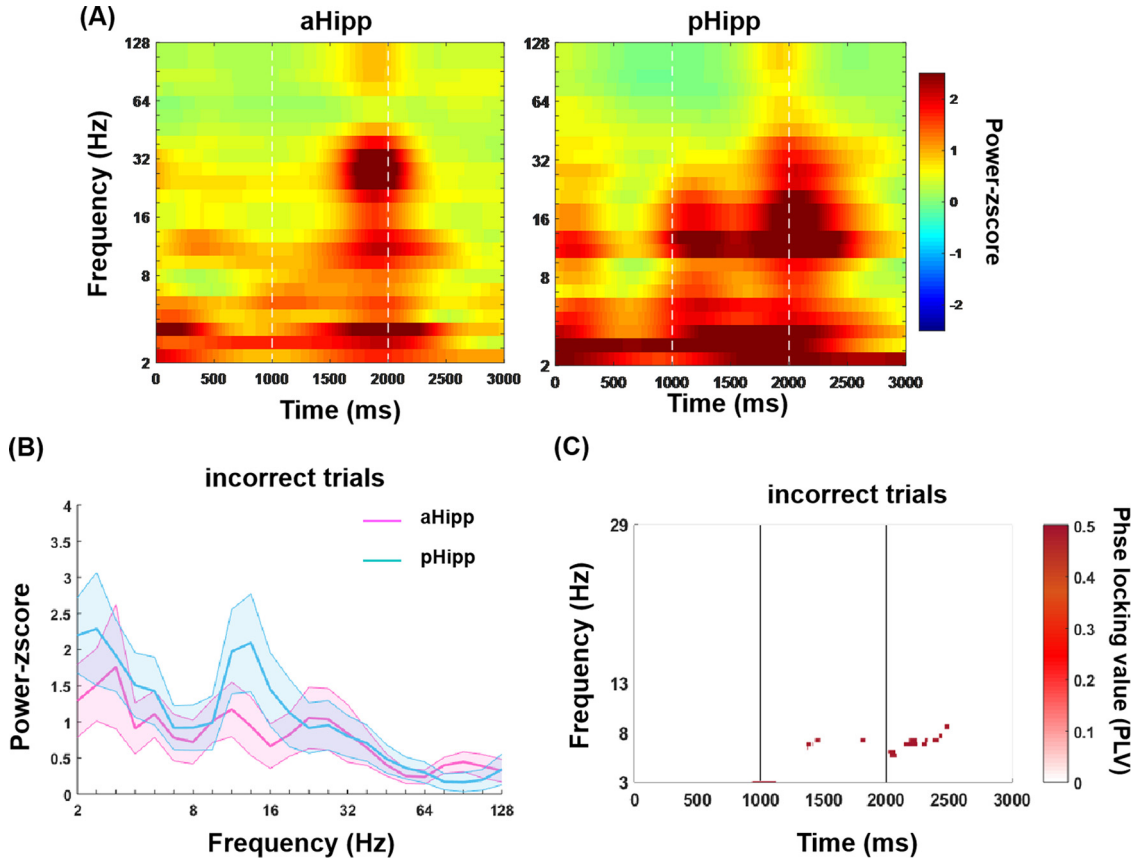

Figure 5. Power and phase synchrony for the incorrect trials. ***A***, Average task-induced power across all subjects during maintenance for the incorrect trials, grouped in the anterior (left column) and posterior hippocampus (right column). Warmer colors denote task-increased power from the baseline and colder colors denote task-decreased power. Task-induced effects on both the aHipp and the pHipp were not sustained during maintenance in the low-frequency range (2–20 Hz; $z < 1.96$) for the incorrect trials. ***B***, Spectral *z*-scored power within the anterior (magenta) and posterior hippocampus (cyan) across all subjects (±SEM shown as shading around the mean trace) for the incorrect trials. The spectral power was not significant ($z < 1.96$) during maintenance, and no significant difference ($p > 0.05$, clustered-based permutation test) was found between the two subregions across the frequency band. ***C***, Significant PLVs above the thresholds ($p < 0.05$. permutation test) across the time–frequency domain were present between the aHipp and the pHipp for the incorrect trials. Only a few scattered points survived testing for incorrect trials. Therefore, the PLV of incorrect trials was not further analyzed.

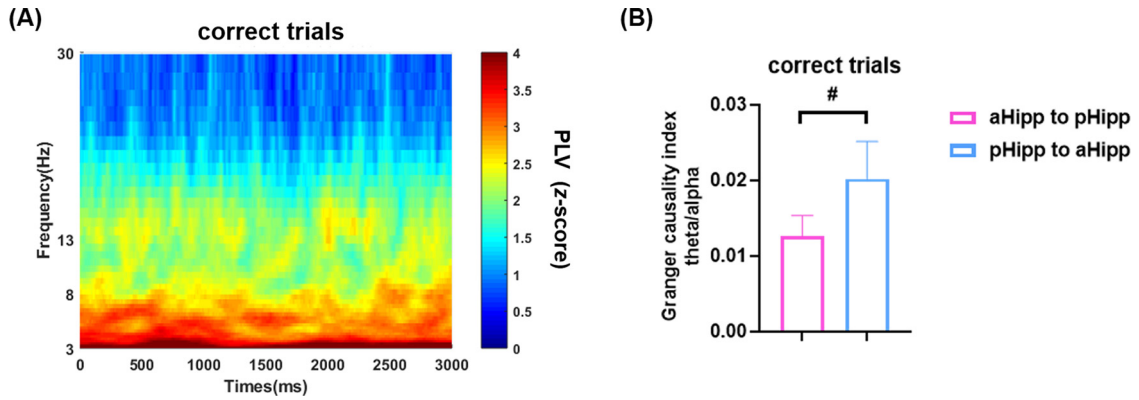

Figure 6. PLV and GC analyses with a bipolar reference. ***A***, Average phase synchronization (*z*-scored PLV) across electrode pairs for the correct trials, with a bipolar reference. Elevated PLV in the low-frequency band was sustained throughout the entire maintenance period. ***B***, Granger causality between hippocampal subregions from both directions by using a bipolar reference for the correct trials. #$p < 0.1$. GC values from the pHipp to aHipp are higher than those in the opposite direction with a trend toward statistical significance (mixed-effect model, $p = 0.092$).

entire maintenance period (Fig. 6*A*). Then, we found higher GC values from the pHipp to aHipp than those in the opposite direction, with a trend toward statistical significance (mixed-effect model, $p = 0.092$) for the correct trials (Fig. 6*B*) and no significant difference between the two directions (mixed-effect model, $p > 0.05$) for the incorrect trials. These findings are consistent with what we observed by using a common reference. In addition, the following findings speak against volume conduction: (1) there was a strong frequency dependence of the intrahippocampal PLVs (Fig. 2*A*) and those to scalp EEGs (Boran et al., 2019), while the transfer of signal through tissue by volume conduction is independent of frequency in the range of the iEEG studied here (Nunez and Cutillo, 1995; Miceli et al., 2017); (2) there was a strong task

dependence of GC values (Figs. 2*D*, 4*A*); and (3) GC is highly anisotropic (Figs. 2*D*, 4*A*). In conclusion, while we cannot rule out a contribution of volume conduction in our data, it seems to be small compared with the effects in the PLVs and GC, which were induced by processing the cognitive task.

Recordings in the epileptic seizure onset zone

Our analysis included recordings from electrodes in the seizure onset zone (SOZ). To assess the possible effects of the SOZ on our findings, we compared the hippocampal electrodes within and outside the SOZ. For the power analysis, the task-induced power was not significantly different between the non-SOZ electrodes and the SOZ electrodes ($p = 0.52$). For the connectivity analysis, we separated the electrode pairs into SOZ (at least one SOZ electrode) and non-SOZ (non-SOZ to non-SOZ electrode) pairs. There was no significant difference in the task-related connectivity measures between the SOZ and non-SOZ electrode pairs (PLV analysis, $p = 0.27$; PAC analysis: aHipp–pHipp, $p = 0.62$; pHipp-aHipp, $p = 0.66$; Granger causality analysis: aHipp to pHipp, $p = 0.14$; pHipp to aHipp, $p = 0.40$). Our analysis implicated residual function in the epileptogenic hippocampus. This is consistent with our previous finding of single neurons in the SOZ that responded to this task (Boran et al., 2019) and more general findings suggesting normal physiological responses to cognitive stimuli in the epileptic sites (Liu and Parvizi, 2019).

Discussion

Together, our results indicated that both subregions of the hippocampus were critical for WM processing; they interacted at a specific frequency band and with a directionality pattern to support the maintenance of the WM information. Specifically, WM maintenance depends on coordinated neural oscillations between the aHipp and the pHipp in the theta/alpha band, with a pHipp-driven information transfer in this band, and a higher PAC between the theta/alpha phase of the pHipp entraining the gamma amplitude of the aHipp. The directionality bias in information transfer within the hippocampus occurred exclusively during the correct WM trials.

The task-induced power revealed sustained low-frequency oscillations (including theta and alpha bands) within both the aHipp and the pHipp during the delay interval in which information was to be remembered. The theta and alpha bands are well known frequency bands that play important roles during WM maintenance. The theta rhythm is thought to underlie the organization of WM items (Roux and Uhlhaas, 2014), and theta power increases in the hippocampus reflect the storage component of WM (Brzezicka et al., 2019). Alpha oscillations were suggested to protect working memory maintenance against anticipated distracters (Bonnefond and Jensen, 2012) and increased during WM maintenance (Boran et al., 2019). Our results echo these findings and suggest that increases in theta/alpha power could support hippocampal WM processing by organizing neural activity (theta) and selectively filtering task-relevant information to avoid distracting information (alpha).

We further observed oscillatory phase synchrony between the aHipp and the pHipp predominantly in the theta/alpha range (3–12 Hz) during the retention interval. Only a few studies have studied oscillatory communication along the long axis of the hippocampus by simultaneously recording both areas in awake unrestrained rodents. Specifically, rodent studies reported increased connectivity between the dorsoventral hippocampus during a WM task (Schmidt et al., 2013). Lesion studies showed a disruption in WM accompanied by reduced theta phase coherence in the dorsoventral hippocampus, and pharmacological treatment resulted in both restored WM task performance and reversed abnormal hippocampal dorsoventral connectivity (Cardoso-Cruz et al., 2014). Our results are thus consistent with the animal literature suggesting that the contribution of synchrony between hippocampal subregions along the long axis to WM processing and extended these findings to humans.

Next, we found that the theta/alpha phase of the pHipp entrained the gamma activity of the aHipp and that theta/alpha-driven information flow occurs from the pHipp to the aHipp during the retention interval with subsequent successful WM responses. Intriguingly, this directional pHipp-to-aHipp information flow was only observed in correct trials and was absent in error trials. These results together suggest that the posterior to anterior influence in the theta/alpha band contributes to the successful maintenance of WM. These interregional information transfer dynamics are consistent with the anatomic circuitry showing projections from the dorsal to the more ventral part of the hippocampus (Amaral and Witter, 1989; Ishizuka et al., 1990). The longitudinal axis may be a locus for interaction between various pieces of WM information with longitudinal interneurons orchestrating the information flow (Harland et al., 2018). Human fMRI studies also suggested hierarchical representations of events along the hippocampal long axis with the pHipp representing detail-level events and the aHipp representing overlapping higher-level, multievent representations (Collin et al., 2015; Schlichting et al., 2015). In our research, the participants needed to remember individual letters; therefore, we speculate that there was a greater requirement for detailed representation, so the pHipp led the information transfer to the aHipp.

Together, our findings suggest a hierarchical information flow from the pHipp to the aHipp in theta/alpha oscillations to successfully maintain WM information. By using human iEEG recording and precise hippocampal subregion segmentation, we demonstrated that working memory maintenance depends on the activity of both the aHipp and the pHipp, which is in line with human fMRI findings. In addition, we provide evidence for coordinated neural oscillations between them with a unidirectional influence from the pHipp to the aHipp via theta/alpha oscillations. This echoes findings from rodents in which lesions of the dorsal Hipp, but not the ventral Hipp, led to deficits in working memory (Pothuizen et al., 2004), as well as rodent studies suggesting preferential involvement of cognitive function in the dorsal Hipp and of emotion in the ventral Hipp (Fanselow and Dong, 2010). Together, our work establishes a bridge between cellular-level work in animals and the extensive literature using noninvasive imaging in humans on the functional specialization of subregions within the hippocampus. The observed directional functional connectivity between the dorsal and ventral subregions is well in line with proposed models of hippocampal long-axis organization within discrete domains (Strange et al., 2014).

There are several limitations of the current study. First, only a verbal WM task was used here. This has the advantage of excluding the possibility of explaining the pHipp-dominated information transfer during WM as a preferential involvement of the pHipp in spatial processing. However, the same strength of the current study limits the generalization of our results to WM processing apart from other information, such as space and time. Second, we did not further map the aHipp or pHipp into cytoarchitectural subfields. In addition to the organizational

patterns along the long axis, the hippocampus is composed of cytoarchitecturally different subfields (CA1–4, dentate gyrus, subiculum; Amunts et al., 2005). However, the small number of electrode contacts in the current study (aHipp for each subject: mean, 3.2 ± 1.8; range, 0–6; pHipp for each subject: mean, 6.7 ± 2.2; range, 1–8) limited the investigation of subfield-specific oscillation-based communication. Future studies with a larger sample size are thus needed to consider the information flow between cytoarchitectural subfields.

In summary, our results linked the intrahippocampal theta/alpha band interaction to WM maintenance and showed that directional information flow occurred from the pHipp to the aHipp during the maintenance interval when the subsequent WM responses were correct. These results add to the growing body of literature about the functional organization along the longitudinal axis of the hippocampus. More broadly, this work allows a detailed mechanistic and more direct understanding of WM.

References

Amaral DG, Witter MP (1989) The three-dimensional organization of the hippocampal formation: a review of anatomical data. Neuroscience 31:571–591.

Amunts K, Kedo O, Kindler M, Pieperhoff P, Mohlberg H, Shah NJ, Habel U, Schneider F, Zilles K (2005) Cytoarchitectonic mapping of the human amygdala, hippocampal region and entorhinal cortex: intersubject variability and probability maps. Anat Embryol (Berl) 210:343–352.

Assaneo MF, Ripollés P, Orpella J, Lin WM, de Diego-Balaguer R, Poeppel D (2019) Spontaneous synchronization to speech reveals neural mechanisms facilitating language learning. Nat Neurosci 22:627–632.

Axmacher N, Henseler MM, Jensen O, Weinreich I, Elger CE, Fell J (2010) Cross-frequency coupling supports multi-item working memory in the human hippocampus. Proc Natl Acad Sci U S A 107:3228–3233.

Barnett L, Seth AK (2014) The MVGC multivariate Granger causality toolbox: a new approach to Granger-causal inference. J Neurosci Methods 223:50–68.

Basti A, Pizzella V, Chella F, Romani GL, Nolte G, Marzetti L (2018) Disclosing large-scale directed functional connections in MEG with the multivariate phase slope index. Neuroimage 175:161–175.

Bonnefond M, Jensen O (2012) Alpha oscillations serve to protect working memory maintenance against anticipated distracters. Curr Biol 22:1969–1974.

Boran E, Fedele T, Klaver P, Hilfiker P, Stieglitz L, Grunwald T, Sarnthein J (2019) Persistent hippocampal neural firing and hippocampal-cortical coupling predict verbal working memory load. Sci Adv 5:eaav3687.

Boran E, Fedele T, Steiner A, Hilfiker P, Stieglitz L, Grunwald T, Sarnthein J (2020) Dataset of human medial temporal lobe neurons, scalp and intracranial EEG during a verbal working memory task. Sci Data 7:30.

Boran E, Stieglitz L, Sarnthein J (2021) Epileptic high-frequency oscillations in intracranial EEG are not confounded by cognitive tasks. Front Hum Neurosci 15:613125.

Brincat SL, Miller EK (2015) Frequency-specific hippocampal-prefrontal interactions during associative learning. Nat Neurosci 18:576–581.

Brzezicka A, Kamiński J, Reed CM, Chung JM, Mamelak AN, Rutishauser U (2019) Working memory load-related theta power decreases in dorsolateral prefrontal cortex predict individual differences in performance. J Cogn Neurosci 31:1290–1307.

Canolty RT, Edwards E, Dalal SS, Soltani M, Nagarajan SS, Kirsch HE, Berger MS, Barbaro NM, Knight RT (2006) High gamma power is phase-locked to theta oscillations in human neocortex. Science 313:1626–1628.

Cardoso-Cruz H, Dourado M, Monteiro C, Matos MR, Galhardo V (2014) Activation of dopaminergic D_2/D_3 receptors modulates dorsoventral connectivity in the hippocampus and reverses the impairment of working memory after nerve injury. J Neurosci 34:5861–5873.

Collin SH, Milivojevic B, Doeller CF (2015) Memory hierarchies map onto the hippocampal long axis in humans. Nat Neurosci 18:1562–1564.

Delorme A, Makeig S (2004) EEGLAB: an open source toolbox for analysis of single-trial EEG dynamics including independent component analysis. J Neurosci Methods 134:9–21.

D'Esposito M (2007) From cognitive to neural models of working memory. Philos Trans R Soc Lond B Biol Sci 362:761–772.

Fan L, Li H, Zhuo J, Zhang Y, Wang J, Chen L, Yang Z, Chu C, Xie S, Laird AR, Fox PT, Eickhoff SB, Yu C, Jiang T (2016) The human brainnetome atlas: a new brain atlas based on connectional architecture. Cereb Cortex 26:3508–3526.

Fanselow MS, Dong HW (2010) Are the dorsal and ventral hippocampus functionally distinct structures? Neuron 65:7–19.

Grady CL (2020) Meta-analytic and functional connectivity evidence from functional magnetic resonance imaging for an anterior to posterior gradient of function along the hippocampal axis. Hippocampus 30:456–471.

Harland B, Contreras M, Fellous J-M (2018) A role for the longitudinal axis of the hippocampus in multiscale representations of large and complex spatial environments and mnemonic hierarchies. In: The hippocampus-plasticity and functions, p 67. London: IntechOpen.

Ishizuka N, Weber J, Amaral DG (1990) Organization of intrahippocampal projections originating from CA3 pyramidal cells in the rat. J Comp Neurol 295:580–623.

Johnson EL, Adams JN, Solbakk AK, Endestad T, Larsson PG, Ivanovic J, Meling TR, Lin JJ, Knight RT (2018) Dynamic frontotemporal systems process space and time in working memory. PLoS Biol 16:e2004274.

Johnson EL, Kam JWY, Tzovara A, Knight RT (2020) Insights into human cognition from intracranial EEG: a review of audition, memory, internal cognition, and causality. J Neural Eng 17:051001.

Kamiński J, Sullivan S, Chung JM, Ross IB, Mamelak AN, Rutishauser U (2017) Persistently active neurons in human medial frontal and medial temporal lobe support working memory. Nat Neurosci 20:590–601.

Kamiński J, Brzezicka A, Mamelak AN, Rutishauser U (2020) Combined phase-rate coding by persistently active neurons as a mechanism for maintaining multiple items in working memory in humans. Neuron 106:256–264.e3.

Kornblith S, Quian Quiroga R, Koch C, Fried I, Mormann F (2017) Persistent single-neuron activity during working memory in the human medial temporal lobe. Curr Biol 27:1026–1032.

Kota S, Rugg MD, Lega BC (2020) Hippocampal theta oscillations support successful associative memory formation. J Neurosci 40:9507–9518.

Lee J-J, Kim HJ, Čeko M, Park B-Y, Lee SA, Park H, Roy M, Kim S-G, Wager TD, Woo C-W (2021) A neuroimaging biomarker for sustained experimental and clinical pain. Nat Med 27:174–182.

Lin JJ, Rugg MD, Das S, Stein J, Rizzuto DS, Kahana MJ, Lega BC (2017) Theta band power increases in the posterior hippocampus predict successful episodic memory encoding in humans. Hippocampus 27:1040–1053.

Lin JJ, Umbach G, Rugg MD, Lega B (2019) Gamma oscillations during episodic memory processing provide evidence for functional specialization in the longitudinal axis of the human hippocampus. Hippocampus 29:68–72.

Liu S, Parvizi J (2019) Cognitive refractory state caused by spontaneous epileptic high-frequency oscillations in the human brain. Sci Transl Med 11:eaax7830.

Maris E, Oostenveld R (2007) Nonparametric statistical testing of EEG- and MEG-data. J Neurosci Methods 164:177–190.

Martínez-Cancino R, Heng J, Delorme A, Kreutz-Delgado K, Sotero RC, Makeig S (2019) Measuring transient phase-amplitude coupling using local mutual information. Neuroimage 185:361–378.

Miceli S, Ness TV, Einevoll GT, Schubert D (2017) Impedance spectrum in cortical tissue: implications for propagation of LFP signals on the microscopic level. eNeuro 4:ENEURO.0291-16.2016.

Miller EK, Lundqvist M, Bastos AM (2018) Working memory 2.0. Neuron 100:463–475.

Nunez PL, Cutillo BA (1995) Neocortical dynamics and human EEG rhythms. Oxford: Oxford UP.

Oostenveld R, Fries P, Maris E, Schoffelen JM (2011) FieldTrip: open source software for advanced analysis of MEG, EEG, and invasive electrophysiological data. Comput Intell Neurosci 2011:156869.

Poppenk J, Evensmoen HR, Moscovitch M, Nadel L (2013) Long-axis specialization of the human hippocampus. Trends Cogn Sci 17:230–240.

Pothuizen HH, Zhang WN, Jongen- Rêlo AL, Feldon J, Yee BK (2004) Dissociation of function between the dorsal and the ventral hippocampus in spatial learning abilities of the rat: a within-subject, within-task comparison of reference and working spatial memory. Eur J Neurosci 19:705–712.

Roux F, Uhlhaas PJ (2014) Working memory and neural oscillations: α-γ versus θ-γ codes for distinct WM information? Trends Cogn Sci 18:16–25.

Schlichting ML, Mumford JA, Preston AR (2015) Learning-related representational changes reveal dissociable integration and separation signatures in the hippocampus and prefrontal cortex. Nat Commun 6:8151.

Schmidt B, Hinman JR, Jacobson TK, Szkudlarek E, Argraves M, Escabí MA, Markus EJ (2013) Dissociation between dorsal and ventral hippocampal theta oscillations during decision-making. J Neurosci 33:6212–6224.

Solomon EA, Stein JM, Das S, Gorniak R, Sperling MR, Worrell G, Inman CS, Tan RJ, Jobst BC, Rizzuto DS, Kahana MJ (2019) Dynamic theta networks in the human medial temporal lobe support episodic memory. Curr Biol 29:1100–1111.e4.

Stolk A, Griffin S, van der Meij R, Dewar C, Saez I, Lin JJ, Piantoni G, Schoffelen JM, Knight RT, Oostenveld R (2018) Integrated analysis of anatomical and electrophysiological human intracranial data. Nat Protoc 13:1699–1723.

Strange BA, Witter MP, Lein ES, Moser EI (2014) Functional organization of the hippocampal longitudinal axis. Nat Rev Neurosci 15:655–669.

Tort AB, Kramer MA, Thorn C, Gibson DJ, Kubota Y, Graybiel AM, Kopell NJ (2008) Dynamic cross-frequency couplings of local field potential oscillations in rat striatum and hippocampus during performance of a T-maze task. Proc Natl Acad Sci U S A 105:20517–20522.

Vogel JW, La Joie R, Grothe MJ, Diaz-Papkovich A, Doyle A, Vachon-Presseau E, Lepage C, Vos de Wael R, Thomas RA, Iturria-Medina Y, Bernhardt B, Rabinovici GD, Evans AC (2020) A molecular gradient along the longitudinal axis of the human hippocampus informs large-scale behavioral systems. Nat Commun 11:960.

Vos de Wael R, Larivière S, Caldairou B, Hong SJ, Margulies DS, Jefferies E, Bernasconi A, Smallwood J, Bernasconi N, Bernhardt BC (2018) Anatomical and microstructural determinants of hippocampal subfield functional connectome embedding. Proc Natl Acad Sci U S A 115:10154–10159.

Wang DX, Schmitt K, Seger S, Davila CE, Lega BC (2021) Cross-regional phase amplitude coupling supports the encoding of episodic memories. Hippocampus 31:481–492.